JOURNAL OF COMPUTATIONAL PHYSICS **123,** 196–206 (1996)
ARTICLE NO. 0016

Stability Analysis of Lattice Boltzmann Methods

JAMES D. STERLING

Advanced Projects Research Incorporated, 2521 Wildrose Lane, Upland, California 91784 and Jet Propulsion Center, MS 301-46, California Institute of Technology, Pasadena, California 91125

AND

SHIYI CHEN

Theoretical Division, MS-B213, Los Alamos National Laboratory, Los Alamos, New Mexico 87545 and IBM Research Division, T. J. Watson Research Center, P.O. Box 218, Yorktown Heights, New York 10598

Received June 3, 1993; revised June 20, 1995

The lattice Boltzmann equation describes the evolution of the velocity distribution function on a lattice in a manner that macroscopic fluid dynamical behavior is recovered. Although the equation is a derivative of lattice gas automata, it may be interpreted as a Lagrangian finite-difference method for the numerical simulation of the discrete-velocity Boltzmann equation that makes use of a BGK collision operator. As a result, it is not surprising that numerical instability of lattice Boltzmann methods have been frequently encountered by researchers. We present an analysis of the stability of perturbations of the particle populations linearized about equilibrium values corresponding to a constant-density uniform mean flow. The linear stability depends on the following parameters: the distribution of the mass at a site between the different discrete speeds, the BGK relaxation time, the mean velocity, and the wavenumber of the perturbations. This parameter space is too large to compute the complete stability characteristics. We report some stability results for a subset of the parameter space for a 7-velocity hexagonal lattice, a 9-velocity square lattice, and a 15-velocity cubic lattice. Results common to all three lattices are (1) the BGK relaxation time τ must be greater than $\frac{1}{2}$ corresponding to positive shear viscosity, (2) there exists a maximum stable mean velocity for fixed values of the other parameters, and (3) as τ is increased from $\frac{1}{2}$ the maximum stable velocity increases monotonically until some fixed velocity is reached which does not change for larger τ.

1. INTRODUCTION

The lattice Boltzmann (LB) method is a recently developed computational scheme used to model fluids under a variety of flow regimes. As a derivative of lattice gas (LG) automata, the LB method deals with fluid dynamics from the microscopic, kinetic level. However, as with the Boltzmann equation, the LB method describes the evolution of particle populations rather than attempting to follow individual particle motion. Thus, the LB method has the flexibility of traditional particle methods, but it has the numerical character of finite-difference schemes. The physical interpretation of the scheme as consisting of a particle streaming step followed by a collision results in a very simple parallel logic that is well suited for implementation on massively parallel computers. The main advantage of the LB method is that the particle interpretation allows the use of very simple boundary conditions so that the parallel implementation may be used even for complex geometries. For this reason, one of the most successful applications of the LB method has been to simulations of flow through porous media [1, 2].

The development of LG models was based on the observation that macroscopic behavior of fluid flow is not very sensitive to the underlying microscopic physics. Thus, models were developed based on the simplest possible particle microworld that would lead to the incompressible Navier–Stokes equation in the limit of small Knudsen number [3]. The methods successfully modeled incompressible fluid flow but noise associated with the particle microworld necessitated the introduction of some type of averaging procedure such as spatial, temporal, or ensemble averaging to characterize the macroscopic flow. A second difficulty is that LG methods have unphysical equations of state and non-Galilean invariant flow. Finally, the transport coefficients that resulted from the microscopic collision rules were inflexibly limited to small ranges of values [4].

In contrast, the numerical solution of the lattice Boltzmann equation (LBE), as proposed by McNamara and Zanetti [5], neglects individual particle motion resulting in smooth macroscopic behavior. Further simplification of the scheme is achieved by linearizing the collision operator [6]. A particularly simple linearized version of the collision operator makes use of a relaxation towards an equilibrium value using a single relaxation time parameter. The relaxation term is known as the BGK [7] collision operator and has been independently suggested by several authors for

0021-9991/96 $12.00

use with this method [8–10]. Use of this collision operator makes the computations much faster and allows flexibility of the transport coefficients. Particle streaming and collision are explicitly computed by performing a type of ''shift'' operation on the parallel computer to represent the particle streaming followed by a purely local operation for the collision. The microscopic approach of the LB method associates physical quantities with the discretization parameters: the time step is the time between particle collisions and the lattice spacing is the distance a particle travels in one time step. Again, the spirit of the approach is to retain the simplest microscopic description that gives the macroscopic behavior of interest.

Application of a Taylor series expansion of the lattice kinetic equation followed by a Chapman–Enskog expansion results in the typical hierarchy of equations; Euler, Navier–Stokes, Burnett, etc. By selecting the appropriate number of speeds and the appropriate form of the equilibrium distribution function, one may match the equations that result from the LB method with those of traditional kinetic theory to the desired level. Higher level terms that are not matched represent behavior of the lattice gas that differs from a Maxwellian gas.

The most common application of the LB method has been to fluid flow models for which only mass and momentum are conserved. The Chapman–Enskog theory for these models typically yields correct behavior to the Euler level but the Navier–Stokes level is correct only in the incompressible limit. In other words, the incorrect terms become small as the square of the Mach number becomes small. This approach has much in common with explicit ''penalty'' or ''pseudocompressibility'' methods of solving incompressible flows [11–13]. Complete energy-conserving models that yield the correct form of the compressible continuity, momentum, and energy equations have been developed by Alexander, Chen, and Sterling [14], McNamara and Alder [15], Qian and Orszag [16], and Chen *et al.* [17]. We note that for any of the LB models, the transport coefficients depend on the time step and lattice spacing. Another way of looking at this is that there is a ''lattice viscosity'' or ''numerical viscosity'' that becomes small as the grid is refined (i.e., time step reduced for fixed particle velocities). This brings us to an alternative view that the higher order terms in the Taylor series expansion of the kinetic equation are not ''physical'' but may be considered ''truncation error'' of a finite difference approximation to some continuous equation.

Indeed, an alternative view of the LB method is that it is a particular space and time discretization of the discrete-velocity Boltzmann equations. These equations are partial differential equations (i.e., continuous in space and time) that describe the evolution of particle populations that have discrete speeds. Researchers have used a variety of discrete-velocity models: models with a single speed were originally developed by Broadwell [18] and recent work by Inamuro and Sturtevant [19] includes many speeds. Inamuro and Sturtevant used first, second, and third order upwind finite difference discretizations of the discrete-velocity Boltzmann equation to study shock-wave structure, conductive heat transfer, and chemical vapor deposition. However, they made use of a large velocity set that was nearly Maxwellian in distribution and since their intention was to model rarefied flows, no Chapman–Enskog procedure was used to assess continuum–limit behavior. More recently, Nadiga and Pullin [20] have implemented a finite volume numerical method to simulate discrete-velocity gases using collisions that achieve local thermodynamic equilibrium.

In contrast to these compressible methods, Reider and Sterling [21] have studied the convergence behavior of different finite-difference approximations to the discrete-Boltzmann equation for velocity sets that provide Navier–Stokes behavior in the incompressible and continuum limits. Ancona [22] introduced the view that the LB method is a finite-difference method for the solution of the macroscopic equations and generalized the method to include fully Lagrangian methods for the solution of partial differential equations.

In traditional kinetic theory, the equilibrium velocity distribution function is the maximum entropy state. Thus, any initial state will evolve towards a state of higher entropy. This result is known as Boltzmann's H-theorem which ensures an increase of entropy, and ensures stability. An H-theorem has been derived for some particle methods and a derivation for lattice gases is included in Ref. [23]. If one can guarantee that the equilibrium distribution function for LB methods is the maximum entropy state, then stability can be guaranteed even though LB approaches are not particle methods [24]. The problem with this approach, however, is that one cannot usually find an equilibrium distribution function that can simultaneously guarantee an H-theorem and allow the correct form of the equations to be obtained. In this paper, we limit our discussion to LB schemes that have been developed for simulating the incompressible Navier–Stokes equations (i.e., simulation in the low Knudsen number and low Mach number limits). These schemes do not have an H-theorem and are therefore subject to numerical instability. Lattice Boltzmann results that are reported in the literature have typically been performed under conditions that provide stable behavior. However, it is well known among LB researchers that instability problems arise frequently. When the LB method is viewed as a finite-difference method for solving the continuum discrete-velocity Boltzmann equations, it becomes clear that numerical accuracy and stability issues should be addressed.

In Section 2 the Chapman–Enskog procedure applied to the continuum discrete-velocity Boltzmann equation is

reviewed and the macroscopic equations corresponding to a 7-velocity hexagonal lattice model are presented. Section 2 also introduces the new interpretation of the lattice Boltzmann method as a particular discretization of the continuum discrete-velocity Boltzmann equations. With this interpretation of the LB method, it is clear that a traditional stability analysis is needed instead of entropy/H-theorem approaches that prove useful for particle methods. In Section 4 we present the von Neumann stability analysis of the lattice Boltzmann method for a uniform flow and report results for the 7-velocity hexagonal lattice, a 9-velocity square lattice, and a 15-velocity cubic lattice. We conclude with some comments concerning the interpretation of the stability results and comparison with other CFD stability criteria.

2. THE LATTICE BOLTZMANN METHOD

This section provides a description of the Chapman–Enskog expansion of the discrete-velocity Boltzmann equation and application of the lattice Boltzmann discretization. The resulting LB method makes use of the following definitions and conditions:

(1) The particle populations f may only move with velocities that are members of the set of discrete velocity vectors $\mathbf{e}_i$. The corresponding populations are denoted f_i.

(2) A collision operator with a single relaxation time, τ, is used to redistribute populations f_i towards equilibrium values f_i^{eq}. This is also referred to as a BGK collision operator where τ is inversely proportional to density [25]. For constant density flows τ is a constant.

(3) The equilibrium velocity distribution function is written as a truncated power series in the macroscopic flow velocity.

The discrete velocity Boltzmann equation then becomes

$$\frac{\partial f_i}{\partial t} + \mathbf{e}_i \cdot \nabla f_i = -\frac{1}{\tau}(f_i - f_i^{\mathrm{eq}}), \tag{1}$$

where the velocity distribution function f_i is constructed so that macroscopic flow variables are defined by its moments:

Mass,

$$n \equiv \sum_i f_i; \tag{2}$$

Momentum,

$$n\mathbf{u} \equiv \sum_i f_i \mathbf{e}_i. \tag{3}$$

Equation (1) may be written in nondimensional form by using a characteristic flow length scale L, reference speed e_r, and density n_r. Two reference time scales are used, t_c to represent the time between particle collisions and L/e_r to represent a characteristic flow time. The reference speed may be selected to be the magnitude of the minimum nonzero discrete velocity. If only one speed is used, then the velocity set for the nondimensional equations is simply a set of unit vectors. The resulting nondimensional equation is

$$\frac{\partial \hat{f}_i}{\partial \hat{t}} + \hat{\mathbf{e}}_i \cdot \hat{\nabla} \hat{f}_i = -\frac{1}{\varepsilon \hat{\tau}}(\hat{f}_i - \hat{f}_i^{\mathrm{eq}}), \tag{4}$$

where the caret symbol is used to denote non-dimensional quantities $\hat{\mathbf{e}}_i = \mathbf{e}_i/e_r$, $\hat{\nabla} = L\nabla$, $\hat{t} = te_r/L$, $\hat{\tau} = \tau/t_c$, and $\hat{f}_i = f_i/n_r$. The parameter $\varepsilon = t_c e_r/L$ and may be interpreted as either the ratio of collision time to flow time or as the ratio of mean free path to the characteristic flow length (i.e., Knudsen number). We will not use the caret notation further but will assume that the equations are in nondimensional form henceforth.

Application of the Chapman–Enskog method to these equations results in the long wavelength governing equations. This method requires the expansion of the distribution function in the small parameter ε such that $f_i = f_i^{(0)} + \varepsilon f_i^{(1)} + \varepsilon^2 f_i^{(2)} + \cdots$, and $f_i^{(0)}$ is identified as $f_i^{(\mathrm{eq})}$ and the remaining terms can be referred to as $f_i^{(\mathrm{neq})}$. The continuity or mass conservation equation to first order in ε is

$$\frac{\partial n}{\partial t} + \nabla \cdot (n\mathbf{u}) = 0, \tag{5}$$

and the momentum equation to first order in ε is

$$\frac{\partial}{\partial t}(n\mathbf{u}) + \nabla \cdot (\mathbf{\Pi}^{(0)} + \mathbf{\Pi}^{(1)}) = 0, \tag{6}$$

where $\mathbf{\Pi}^{(l)}$ is the momentum flux tensor and is defined as

$$\mathbf{\Pi}_{\alpha\beta}^{(l)} = \sum_i e_{i\alpha} e_{i\beta} f_i^{(l)}, \tag{7}$$

for $l = 0, 1$. The constitutive relations for this tensor are obtained by selecting a particular lattice geometry and equilibrium distribution functional form and then proceeding to match moments of the distribution function with terms in the Navier–Stokes equations.

As an example, when this is performed for a hexagonal lattice with unit velocity vectors defined by $\mathbf{e}_i = \{\cos(2\pi$

$(i-1)/6)$, $\sin(2\pi(i-1)/6)\}$ for $i = 1, 2, ..., 6$, a suitable equilibrium distribution function is found to be

$$f_0^{\text{eq}} = n\alpha - nu^2 \tag{8}$$

$$f_i^{\text{eq}} = \frac{n(1-\alpha)}{6} + \frac{n}{3}\mathbf{e}_i \cdot \mathbf{u} + \frac{2n}{3}(\mathbf{e}_i \cdot \mathbf{u})^2 - \frac{n}{6}u^2, \tag{9}$$

where α is a constant that determines the distribution of mass between the moving and nonmoving populations [26].

The momentum flux tensor for this distribution function is obtained by substituting Eq. (9) into Eq. (7). The resulting expression for $\mathbf{\Pi}^{(0)}$ is

$$\mathbf{\Pi}_{\alpha\beta}^{(0)} = 3n\frac{1-\alpha}{6}\delta_{\alpha\beta} + nu_\alpha u_\beta, \tag{10}$$

which gives a Galilean invariant convective term in the momentum equation. By identifying the isotropic part of this tensor as the pressure, we obtain an ideal gas law equation of state (i.e., $p = ((1-\alpha)/2)n$) and the gradient of the pressure in the momentum equation. Similarly, evaluation of $\mathbf{\Pi}^{(1)}$ using standard Chapman–Enskog procedure results in the final form of the momentum equation;

$$\begin{aligned} n\frac{\partial u_\alpha}{\partial t} + nu_\beta\frac{\partial u_\alpha}{\partial x_\beta} &= -\frac{\partial p}{\partial x_\alpha} + \frac{\partial}{\partial x_\beta}\left(\frac{\lambda}{n}\left(\frac{\partial nu_\gamma}{\partial x_\gamma}\delta_{\alpha\beta} + u_\alpha\frac{\partial n}{\partial x_\beta} + u_\beta\frac{\partial n}{\partial x_\alpha}\right)\right) \\ &\quad + \frac{\partial}{\partial x_\beta}\left(\mu\left(\frac{\partial u_\beta}{\partial x_\alpha} + \frac{\partial u_\alpha}{\partial x_\beta}\right)\right), \end{aligned} \tag{11}$$

where

$$\mu = \tau n/4 \tag{12}$$

and

$$\lambda = \frac{\tau n(2\alpha-1)}{4}. \tag{13}$$

In two dimensions, the bulk viscosity is the sum of these two so that

$$K = \frac{\tau n\alpha}{2}, \tag{14}$$

which gives zero bulk viscosity as expected for the monatomic gas when energy is conserved (i.e., when $\alpha = 0$ it can be shown that conservation of mass is equivalent to conservation of energy).

Note that these equations are not the standard Navier–Stokes equations because there are derivatives of the density in the second viscosity term on the right side of the equation. If these gradients of density are negligible this hexagonal lattice, discrete Boltzmann equation should behave approximately as the Navier–Stokes equations. Since the gradients of the density are $O(u^2)$ (see Ref. [27, 28]), the unphysical terms in Eq. (11) are $O(u^3)$. Thus, although the physics contains compressibility effects (that differ from the compressible Navier–Stokes equations), one may come arbitrarily close to solving incompressible flow by reducing the Mach number and thereby allowing information to propagate throughout the domain while little convection occurs. For this reason, no Poisson solver is required to determine the pressure and simple particle reflections at boundaries may be used to invoke no-slip conditions. We also note that if the second viscosity λ is zero, the complete compressible Navier–Stokes equations are given, but the bulk viscosity is then nonzero.

There are differences between the incompressible Navier–Stokes equations and the macroscopic behavior of the discrete-velocity Boltzmann equations because of the asymptotic nature of the Chapman–Enskog method. The differences may be attributed to Burnett level and higher level terms or as small deviations from the above relation for the kinematic viscosity. For this reason, previous LB studies have reported comparisons between the Chapman–Enskog prediction and numerical simulation measurements of the viscosity (e.g., Kadanoff *et al.* [29]). However, the Burnett level terms are expected to become negligible as the global Knudsen number becomes small. Since the Knudsen number is proportional to the Mach number divided by the Reynolds number, the Burnett terms may be classified with other ''compressibility'' effects and should become small as the Mach number approaches zero for a fixed Reynolds number.

Thus, the discrete Boltzmann equation in dimensionless form, Eq. (4), may be discretized and numerically simulated to provide approximate solution to the continuity and momentum equations given by Eqs. (5) and (11), respectively. The results can then be put back into dimensional form using the reference quantities. Simulations may come arbitrarily close to incompressible Navier–Stokes behavior with differences being attributed solely to discretization and compressibility effects.

At this point we will narrow our view to a particular discretization of the non-dimensional discrete Boltzmann equation. In particular, we will choose the lattice-Boltzmann method which is an exact Lagrangian solution for the convective derivatives. For a given convection velocity,

this type of scheme is typically obtained by using an Euler time step in conjunction with an upwind spatial discretization and then setting the grid spacing divided by the time step equal to the velocity. Discretization of Eq. (4) results in the equation

$$\frac{f_i(\mathbf{x}, t+\Delta t) - f_i(\mathbf{x}, t)}{\Delta t} + \frac{f_i(\mathbf{x}+\mathbf{e}_i\,\Delta x, t+\Delta t) - f_i(\mathbf{x}, t+\Delta t)}{\Delta x} = -\frac{(f_i\mathbf{x}, t) - f_i^{(0)}(\mathbf{x}, t))}{\varepsilon\tau}. \tag{15}$$

Lagrangian behavior is then obtained by the selection of the lattice spacing divided by the time step to equal the magnitude of $\mathbf{e}_i$, which was normalized so that the smallest velocity magnitude is unity. When the equation is multiplied by Δt, the result is the cancellation of two terms on the left side of the above equation, leaving only one term evaluated at $t + \Delta t$ so that the method is explicit.

The next characteristic of the lattice Boltzmann method is the selection of the time step to equal the reference collision time ($\Delta t = t_c$). The result is the cancellation of the Knudsen number in the denominator of the collision term giving the following simple form that is commonly referred to as the lattice Boltzmann equation (LBE),

$$f_i(\mathbf{x} + \mathbf{e}_i\,\Delta t, t + \Delta t) - f_i(\mathbf{x}, t) = -\frac{1}{\tau}(f_i(\mathbf{x}, t) - f_i^{(0)}(\mathbf{x}, t)). \tag{16}$$

This equation has a particularly simple physical interpretation in which the collision term is evaluated locally and there is only one streaming step or ''shift'' operation per lattice velocity. This stream-and-collide particle interpretation is a result of the fully Lagrangian character of the equation for which the lattice spacing is the distance travelled by the particles during a time step. Higher order discretizations of the discrete Boltzmann equation typically require several ''shift'' operations for the evaluation of each derivative and a particle interpretation is less obvious. In fact, the entire derivation of the LB method was originally based on the idea of generalizing LG models by solving the LG Boltzmann equation and relaxing the exclusion principle that particle populations be either zero or one for each velocity [5]. It did not originally occur to the authors that the LB method could be considered a particular discretization for the discrete Boltzmann equation [30].

The particle model allows boundary conditions to be implemented as particular types of collisions. If populations are reflected directly back along the lattice vector along which they streamed, the result is a ''no-slip'' velocity boundary condition. One may also define specular reflection conditions that yield a slip condition. Models for which energy is conserved allow specification of heat-transfer boundary conditions using particle reflection conditions as well [14]. These simple boundary conditions make the LB method particularly suited to parallel computing environments and the simulation of flows in complex geometries.

Although first-order discretizations have been used, the LB method is second order in both space and time when contributions that result from discretization error are taken to represent physics [21, 22]. The inclusion of this numerical viscosity is accomplished by Taylor expanding Eq. (16) about x and t. When the second-order terms in this expansion are included in the above Chapman–Enskog analysis, the result is that the coefficient τ in the transport coefficients is simply replaced by $\tau - \frac{1}{2}$ (see Ref. [14]). Thus, the lattice contribution to the viscosity for this LB scheme is negative, requiring the value of the relaxation time to be greater than half the time step to maintain positive viscosity. Note that third-order terms in the Taylor-series expansion are necessarily of order ε^2 in the Chapman–Enskog expansion. Thus, as with traditional kinetic theory, there may be some error arising from the Burnett level terms.

Since the LB method under consideration is valid only in the incompressible limit, the main dimensionless parameter of interest is the Reynolds number. Convergence of the solution to the incompressible Navier–Stokes equations for a fixed Reynolds number is then obtained by letting the Mach number become small enough to remove compressibility effects and by letting the lattice spacing $e_r\,\Delta t$ become small enough to ''resolve'' the flow. Reverting to the caret notation for dimensionless quantities, the Reynold's number for the hexagonal lattice may now be written

$$\mathrm{Re} = \frac{LU}{\nu} = \frac{4N\hat{U}}{\hat{\tau} - 1/2}, \tag{17}$$

where $N = L/\Delta x$ is the number of lattice spaces. The dimensionless velocity is the characteristic Mach number ($\hat{U} = U/e_r$) which should be small to simulate incompressible flow. Thus, the convergence at a given Reynolds number is performed by increasing N while either increasing $\hat{\tau}$ and/or decreasing $\hat{U}$ appropriately. For a decrease in the value of $\hat{U}$, a proportionate increase in the number of time steps is needed to reach the same flow evolution time.

Concluding, the LB method makes use of first order discretizations of the dimensionless discrete velocity Boltzmann equation in both time and space. The dimensionless time step and lattice spacing are set equal and numerical contributions to viscosity are accounted for and considered to be part of the physics of the method. With these effects

included, the LB method is a second order method in both space and time but in the case of LB models developed for incompressible Navier–Stokes simulation, care must be taken to ensure that the Mach number is small enough that the deviation from incompressible behavior is negligible.

3. LATTICE BOLTZMANN LINEAR STABILITY

3.1. *Theory Development*

The lattice Boltzmann equation, Eq. (16), is an explicit scheme for the computation of the particle population associated with each discrete velocity. It is a nonlinear scheme due to the use of the equilibrium distribution function in the collision term. This function is quadratic in velocity (cubic for energy conserving models) and the density and velocity are computed as sums over all of the populations at a site. In an effort to assess the numerical stability of LB schemes with a linearized collision operator, Benzi *et. al.* [31] and Grunau [32] performed stability analyses by neglecting nonlinear terms. Their linear analysis is equivalent to studying the stability under conditions of zero mean flow. They have shown that the stability in such cases is wavenumber independent and is therefore determined by the collision operator alone.

In contrast, we consider a von Neumann linearized stability analysis of the LB scheme that includes the linearization of all nonlinear terms about global equilibrium values of the populations (denoted by the overbar) that are based on some mean density, velocity, and internal energy for energy-conserving models. Thus, we expand f_i as

$$f_i(x,t) = \overline{f_i^{(0)}} + f_i'(x,t), \tag{18}$$

where the global equilibrium populations $\overline{f_i^{(0)}}$ are constants that do not vary in space or time and depend only on the mean density and velocity. The fluctuating quantities f_i' are not equal to $f_i^{(\mathrm{neq})}$ because we have linearized about the equilibrium populations evaluated for a mean density and mean velocity. However, the density and velocity deviate from the mean values such that the local equilibrium populations vary in space and time. These compressible disturbances are appropriate for stability studies of both pseudocompressiblity LB methods and energy-conserving, fully compressible LB methods. If the perturbations are uniform in space, $f_i' = f_i^{(\mathrm{neq})}$ and we recover the stability results for the collision term alone.

We define the update operator for populations f_i to be

$$g_i(f_j) = f_i(\mathbf{x},t) - \frac{1}{\tau}\left(f_i(\mathbf{x},t) - f_i^{(0)}(\mathbf{x},t)\right), \tag{19}$$

where all of the j populations at a site enter through the equilibrium distribution function on the right side of the equation. Taylor expanding g about $\overline{f_i^{(0)}}$ results in the following equation:

$$\begin{aligned}\overline{f_i^{(0)}} + f_i'(\mathbf{x} + \mathbf{e}_i\Delta t, t + \Delta t) \\ = g_i(\overline{f_j^{(0)}}) + \frac{\partial g_i(\overline{f_j^{(0)}})}{\partial f_j} f_j'(x,t) + O(f_j'(x,t)^2).\end{aligned} \tag{20}$$

Since $\overline{f_i^{(0)}} = g_i(\overline{f_j^{(0)}})$, the resulting linearized system is

$$f_i'(\mathbf{x} + \mathbf{e}_i\Delta t, t + \Delta t) = G_{ij} f_j'(x,t), \tag{21}$$

where G_{ij} is the Jacobian matrix corresponding to the coefficient of the linear term in Eq. (20) and does not depend on location or time.

Spatial dependence of the stability is investigated by taking the Fourier transform of Eq. (21) to obtain

$$F_i(\mathbf{k}, t + \Delta t) = \Gamma_{ij} F_j(\mathbf{k}, t), \tag{22}$$

where

$$\Gamma_{ij} = \mathrm{diag}\{\exp(-i\mathbf{k}\cdot\mathbf{e}_i\Delta t)\}G_{ij}, \tag{23}$$

and the wavenumber has units of inverse lattice spacing. These units are not the most common form for presentation: if we define wavenumber using $\exp(-2\pi i\mathbf{k}\cdot\mathbf{e}_i\Delta t)$, then k is the number of sine waves in the domain and the highest resolution wavenumber is $1/(2\Delta x)$.

We observe that if the wavenumber is zero, the first matrix becomes the identity matrix and the eigenvalues of G_{ij} determine stability. In this case of uniform flow, if the eigenvalues of G_{ij} have modulus less than unity, then the scheme is asymptotically stable. The eigenvalues are $\{1, 1 - 1/\tau\}$, where the unity eigenvalues have multiplicity $D + 1$ in D dimensions, corresponding to microscopic mass and momentum conservation. Thus, stability of uniform flows is guaranteed if $\tau > \frac{1}{2}$.

The elements of the matrix G_{ij} include the linearization of the nonlinear terms in the equilibrium distribution function. As an example, the derivative with respect to f_j of the first nonlinear term in velocity of the equilibrium distribution function, $n(\mathbf{e}_i\cdot\mathbf{u})^2$ is

$$2(\mathbf{e}_i\cdot\mathbf{e}_j)(\mathbf{e}_i\cdot\bar{\mathbf{u}}) - (\mathbf{e}_i\cdot\bar{\mathbf{u}})^2. \tag{24}$$

Stability has been investigated by using *Mathematica*™ version 1.2 to solve for eigenvalues of Γ_{ij} both algebraically and numerically for several lattices and associated equilibria. The following sections document the stability boundaries as functions of the following five parameters; wave-

number $\mathbf{k}$, relaxation parameter τ, velocity $\bar{\mathbf{u}}$, and particle population distribution parameters α and β (introduced for square and cubic lattices below).

3.2. *Seven-Velocity Hexagonal Lattice Results*

The lattice definition and equilibrium velocity distribution function for the hexagonal lattice is described in Section 2 above. When the lattice Boltzmann equation is linearized about a mean velocity and density, and a Fourier transform is performed, the eigenvalues of the resulting Jacobian matrix Γ_{ij} may be evaluated to assess linear stability of the system. As mentioned above, if the wavenumber is zero, $\tau = \frac{1}{2}$ is the only linear stability boundary. Indeed, numerical simulation results are consistently unstable if the value of τ is too close to 0.5. This boundary has been well tested because there is considerable interest in using this LB method to simulate high-Reynolds number flow and as τ appoaches 0.5, the Reynolds number approaches infinity. The fact that values of τ slightly greater than one-half can lead to instability is attributed to the nonlinear terms in the equilibrium distribution function.

The linearized stability in the hexagonal case depends on the four parameters $\tau, \alpha, \bar{\mathbf{u}}$, and $\mathbf{k}$. Therefore, a complete mapping of all stability boundaries is not computationally feasible for even this seven-velocity model. Since the velocity and wavenumber are both vectors, a study was performed in which the angle between these vectors was varied while the other parameters remained fixed. The result for the case studied was that the most unstable condition occurred when the angle between the vectors was equal to zero. Although there is no proof that this result holds for all parameter values, we have assumed that the velocity and the wavenumber vectors are aligned with the first velocity vector for each lattice (i.e., the horizontal axis). This assumption was made for all of the results that follow.

The second attempt at simplifying the analysis was to determine if there was a single wavenumber that was consistently the most unstable. When using a unit lattice spacing, the highest resolvable wavenumber is equal to π. Figure 1 is a plot of the maximum eigenvalue magnitude of Γ_{ij} as a function of wavenumber for two unstable conditions when $\tau = 0.5$. The solid line corresponds to $\bar{\mathbf{u}} = 0.2$ and $\alpha = 0.2$ and the dotted line is for $\bar{\mathbf{u}} = 0.23$ and $\alpha = 0.3$. In the first case the most unstable wavenumber is near π and in the second case it is near 1.9. Thus, there is not a single wavenumber that is always the most unstable and therefore, in subsequent studies we evaluated eigenvalues at wavenumbers from 0.1 to 3.1 in steps of 0.2 and the wavenumber with the largest eigenvalue modulus was considered to be the "most unstable wavenumber." This coarse wavenumber resolution undoubtedly results in stability boundaries that are actually in an unstable parameter range. In other words, stability boundaries in the following

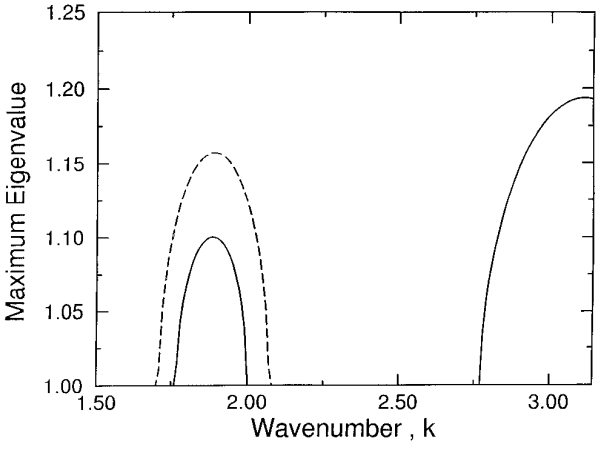

FIG. 1. Hexagonal lattice maximum eigenvalue magnitude as function of wavenumber for $\tau = 0.5$ for two cases. Dashed line is for $\alpha = 0.3$ and $\bar{\mathbf{u}} = 0.23$. Solid line is for $\alpha = 0.2$ and $\bar{\mathbf{u}} = 0.2$.

results should be shifted slightly towards the stable parameter domain.

The distribution of the mass between the nonmoving population and the six moving populations is controlled by the parameter α. Since we are usually interested in high-Reynolds number flows, we investigated the stability of the method as a function of α and $\bar{\mathbf{u}}$ when $\tau = \frac{1}{2}$. An iterative scheme was used in which a value of α was selected and $\bar{\mathbf{u}}$ was incrementally increased until the maximum eigenvalue modulus exceeded unity. The neutral stability boundary was obtained in this manner by varying the value of α from zero (equivalent to an energy-conserving model) to near unity (for which almost all of the mass is stationary). The resulting boundary is plotted as the left curve in Fig.

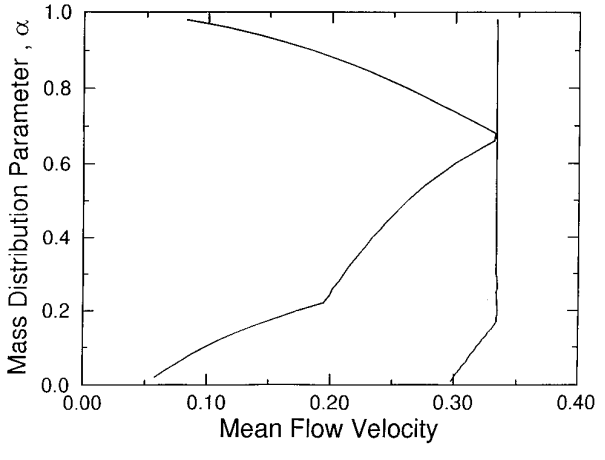

FIG. 2. Stability boundaries as function of $\bar{\mathbf{u}}$ and α for most unstable wavenumber for $\tau = 0.5$. The left curve is the neutral stability boundary for the hexagonal lattice. The right curve is the neutral stability curve for the square lattice for mass distribution parameters related by $\beta = 1/4 - \alpha/3$.

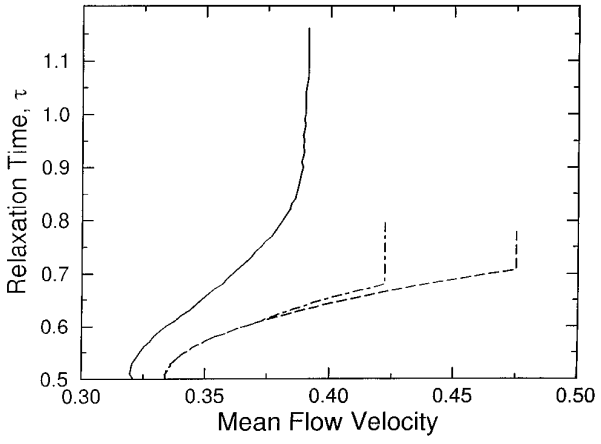

FIG. 3. Stability boundaries as function of $\bar{\mathbf{u}}$ and τ for most unstable wavenumber. The solid line is the neutral stability curve for the hexagonal lattice for $\alpha = 0.7$. The middle curve (dash-dot) is the neutral stability curve for the square lattice for $\alpha = \frac{4}{9}$ and $\beta = \frac{1}{9}$. The dashed curve is the neutral stability curve for the cubic lattice for $\alpha = \frac{1}{8}$ and $\beta = 0.1625$.

2. As the value of α is increased from near zero, the velocity for which the LB scheme is stable increases to a maximum of around one-third when α is near two-thirds. As α increases further, however, the maximum stable velocity again decreases. The data in Fig. 1 were taken near the kink in the stability boundary curve near $\bar{\mathbf{u}} = 0.2$. The kinks are caused when a parameter change results in the most unstable wavenumber shifting to a different eigenvalue.

It is well known from simulations that as τ is increased, the LB method becomes stable at higher values of velocity for a given value of α. A study of this effect was performed by selecting $\alpha = 0.7$ (near the most stable value in Fig. 2) and then iterating the mean flow velocity and the relaxation time to determine the neutral stability boundary. The results are presented in Fig. 3 as the solid curve. When $\tau = \frac{1}{2}$ we see in both Fig. 2 and Fig. 3 that the maximum stable mean flow velocity is near 0.32. As the value of τ increases, the maximum stable velocity is seen to decrease slightly and then increase and level off at a value of about 0.39.

The existence of such a limiting stable velocity is indicative of the inability of the finite set of particle velocities to represent large flow velocities. As the mean velocity increases, the distribution of finite-velocity populations becomes increasingly anisotropic. For small velocities we see that a corresponding increase in the viscosity allows stability to be maintained. However, above the limiting stable velocity, the anisotropy of the population distribution increases in time which decreases entropy in a manner that is characteristic of numerical instability.

Concluding, the maximum velocity should be small to (1) retain a stable scheme and (2) keep higher-order terms from the Chapman–Enskog expansion negligible. Since the velocity is limited, high Reynolds number flow is obtained by either increasing resolution or decreasing τ to values near one-half (i.e., near the linear stability boundary).

3.3. *Nine-Velocity Square Lattice Results*

Another lattice that is commonly used for two-dimensional incompressible flow simulations is the nine-velocity square lattice defined by vectors, $\mathbf{e}_i^{\mathrm{I}} = \{\cos(\pi(i-1)/2), \sin(\pi(i-1)/2)\}$ and $\mathbf{e}_i^{\mathrm{II}} = \{\cos(\pi(i-\frac{1}{2})/2), \sin(\pi(i-\frac{1}{2})/2)\}$ for $i = 1, 4$. The equilibrium distribution function for these moving populations and a nonmoving population is given by

$$f_0^{\mathrm{eq}} = n\alpha - \tfrac{2}{3}nu^2, \tag{25}$$

$$f_i^{\mathrm{I,eq}} = n\beta + \frac{n}{3}\,\mathbf{e}_i^{\mathrm{I}} \cdot \mathbf{u} + \frac{n}{2}\,(\mathbf{e}_i^{\mathrm{I}} \cdot \mathbf{u})^2 - \frac{n}{6}\,u^2 \tag{26}$$

$$f_i^{\mathrm{II,eq}} = n\,\frac{(1 - 4\beta - \alpha)}{4} + \frac{n}{12}\,\mathbf{e}_i^{\mathrm{II}} \cdot \mathbf{u} + \frac{n}{8}\,(\mathbf{e}_i^{\mathrm{II}} \cdot \mathbf{u})^2 - \frac{n}{24}\,u^2. \tag{27}$$

The Jacobian matrix Γ_{ij} for this system is a 9×9 matrix which again gives $\tau = \frac{1}{2}$ as the only stability boundary for homogeneous flow ($\mathbf{k} = 0$). The first numerical study for this lattice was to determine if the most unstable wavenumber occurred at a single value. Unlike the results shown in Fig. 1 for the hexagonal lattice, the most unstable wavenumber was consistently equal to about 2.3 when $\tau = \frac{1}{2}$. It is not obvious why the value of 2.3 was the most unstable wavenumber but it was consistently used in subsequent studies when τ was equal to 0.5.

With both α and β as mass distribution parameters, there are five parameters in the matrix Γ_{ij}. The next numerical study performed on this system addressed the stability for various mass distributions for fixed mean speed and relaxation time for the most unstable wavenumber. The dotted lines in Fig. 4 delineate the stability boundaries when $\tau = 0.5$ and $\mathbf{u} = 0.3$. Combinations of α and β that lie between the two dotted lines result in linear stability while combinations to the left and right of the dotted lines result in linear instability. We note that the values of $\alpha = \frac{4}{9}$ and $\beta = \frac{1}{9}$ used in Ref. [27] lie in the stable domain. Also, these particular values cause the second viscosity to be identically zero ($\lambda = 0$) so that compressible Navier–Stokes equations (5) and (11) are recovered but the bulk viscosity is equal to the shear viscosity.

The strip of stable eigenvalues in Fig. 4 allows us to eliminate the parameter β for subsequent parameter studies by enforcing a parametric relation with α. We originally chose $\beta = \frac{1}{4} - \alpha/3$ to fall within the stable strip of values.

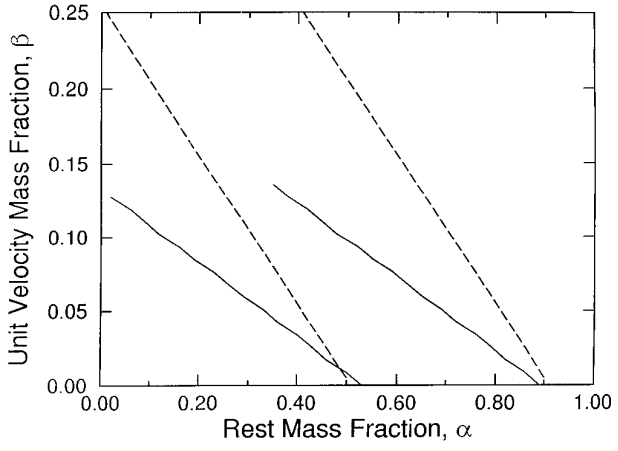

FIG. 4. Stability boundaries as function of mass distribution parameters for most unstable wavenumber for $\tau = 0.5$. The region between the two dotted lines is the stable range for the square lattice for $\bar{\mathbf{u}} = 0.3$. The region between the two solid lines is the stable range for the cubic lattice for $\bar{\mathbf{u}} = 0.32$.

However, this relation plotted as a line on Fig. 4 would lie in the center of the stable range when $\beta = 0$ and $\alpha = \frac{3}{4}$ but when $\beta = \frac{1}{4}$ and $\alpha = 0$ the line would fall just outside the stable range. Nonetheless, this relation was used in the following studies.

The stability boundary for the square lattice is plotted as the right curve in Fig. 2 when the above parametric relation for β is used, $\tau = \frac{1}{2}$, and the most unstable wavenumber is used. From Fig. 4, the parametric relation for β indicates instability for $\mathbf{u} = 0.3$ when $\alpha = 0$. This result can also be seen in Fig. 2 which shows that the neutral stability boundary at $\alpha = 0$ occurs for the velocity just under 0.3. The most interesting result seen in this figure however, is that for values of α greater than about 0.2, the maximum stable velocity is a constant near $\frac{1}{3}$. We have not been able to identify an analytic reason that $\bar{\mathbf{u}} = \frac{1}{3}$ is the stability boundary and is independent of α in the center of the stable parameter strip seen in Fig. 4.

Since the stability is independent of α over a wide range of values, we have used the values of Ref. [27] to study the stability characteristics as the relaxation time is varied. The neutral stability boundary is plotted as the middle curve (dot-dash) in Fig. 3 when $\alpha = \frac{4}{9}$, $\beta = \frac{1}{9}$, and the most unstable wave number (not necessarily 2.3 when τ varies) is considered. The results are similar to the solid curve in Fig. 3 which was discussed in the hexagonal lattice results. As τ is increased from one-half, the maximum stable mean flow velocity increases monotonically from about one-third to a value near 0.42 when τ is near 0.68. However, the maximum stable velocity does not change for further increases of τ. The kink in the curve is a result of the shift of the most unstable eigenvalue/wavenumber to another eigenvalue for which the most unstable wavenumber is $\pi/2$. High Reynolds number flow is obtained by allowing τ to approach the stability boundary of $\tau = \frac{1}{2}$, in accordance with the results for the hexagonal lattice discussed above.

3.4. *Fifteen-Velocity Cubic Lattice Results*

A simple way to extend the square lattice, with vectors to the sides and corners of the square, to three dimensions is to use vectors to the sides and corners of a cube [33, 10, 34]. This defines a body-centered-cubic lattice with $\mathbf{e}_i^{\mathrm{I}} \in (\pm 1, 0, 0), (0, \pm 1, 0), (0, 0, \pm 1)$, and $\mathbf{e}_i^{\mathrm{II}} \in (\pm 1, \pm 1, \pm 1)$. The equilibrium distribution function for these moving populations and a non-moving population is given by

$$f_0^{(\mathrm{eq})} = \alpha n - \frac{n}{2}\mathbf{u}^2, \tag{28}$$

$$f_i^{\mathrm{I},(\mathrm{eq})} = \beta n + \frac{n}{3}(\mathbf{e}_i^{\mathrm{I}} \cdot \mathbf{u}) + \frac{n}{2}(\mathbf{e}_i^{\mathrm{I}} \cdot \mathbf{u})^2 - \frac{n}{6}\mathbf{u}^2, \tag{29}$$

for $\mathbf{e}_i^{\mathrm{I}}$ along the lattice axes, and

$$f_i^{\mathrm{II},(\mathrm{eq})} = \frac{(1 - 6\beta - \alpha)}{8} n + \frac{n}{24}(\mathbf{e}_i^{\mathrm{II}} \cdot \mathbf{u}) + \frac{n}{16}(\mathbf{e}_i^{\mathrm{II}} \cdot \mathbf{u})^2 - \frac{n}{48}\mathbf{u}^2, \tag{30}$$

for $\mathbf{e}_i^{\mathrm{II}}$ along the links to the corners of the cube.

As in the case of the nine-velocity 2D model, the first numerical study performed on this system addressed the determination of the most unstable wavenumber. Because of the similarities in the lattice definitions, the most unstable eigenvalue again occurs at wavenumber equal to 2.3 for unit lattice spacing when $\tau = \frac{1}{2}$.

Following the investigation discussed above for the 2D square lattice, the next investigation studied the dependence of stability on the mass distribution parameters α and β for fixed mean speed and relaxation time for the most unstable wavenumber. The solid lines in Fig. 4 delineate the stability boundaries when $\tau = 0.5$ and $\bar{\mathbf{u}} = 0.32$. Combinations of α and β that lie between the two lines result in linear stability while combinations to the left and right of the dotted lines result in linear instability. Values of $\alpha = \frac{1}{8}$ and $\beta = \frac{1}{8}$ used in Ref. [34] lie near the top and left of the stable domain seen in Fig. 4.

A parametric relation between α and β was chosen to fall along the strip of stable values from Fig. 4. The relation was $\beta = 0.2 - 0.3\alpha$ which lies near the center of the strip for all values (in contrast with the square lattice relation that fell just outside the stable strip for small α values). Using this relation, the following results were similar to those found in the case of the nine-velocity square lattice.

For $\tau = 0.5$, and $\mathbf{k} = 2.3$, the linear stability boundary was computed for varying α and $\bar{\mathbf{u}}$. As in the case of the

2D square lattice, the neutral stability boundary was found to occur for a mean velocity of about one-third independent of α. A plot of this curve would appear as a vertical line on top of the square lattice line in Fig. 2. Finally, a stability boundary was found for $\alpha = \frac{1}{8}$ and the most unstable wavenumber for varying τ and $\bar{\mathbf{u}}$. The resulting stability boundary is plotted as the right curve (dashed) in Fig. 3, verifying that the cubic lattice stability results are very similar to the square lattice results when the mass distribution parameters are selected as discussed above. The main difference is that the cubic lattice has a larger maximum stable mean flow velocity that is near 0.475 for τ above about 0.7.

4. CONCLUSIONS

The lattice Boltzmann equation is viewed as a Lagrangian finite-difference numerical approximation to the discrete-velocity Boltzmann equation that makes use of a BGK collision operator. The collision serves to relax the velocity distribution function towards an equilibrium distribution that is selected so that the first few velocity moments match those of the Maxwell–Boltzmann distribution. Thus, models have been developed for which a Chapman–Enskog expansion predicts second-order numerical accuracy for the solution of the incompressible Navier–Stokes equations. In addition to conserving mass and momentum during collision, the aforementioned matching criteria are also required, with the result that entropy is not necessarily increased during the collision. As a finite difference scheme that does not provide an H-theorem for the particle model, it is not surprising that numerical instability can and frequently does arise during simulation. For this reason, a linearized stability analysis was performed on the hexagonal, square, and cubic lattices defined above.

Linearization of the population f_i is performed about an equlibrium value that does not vary in space or time and depends only on mean density and velocity. We then investigate whether perturbations in the populations grow or decay. The linear stability of the LB models depends on the mass distribution parameters, the mean velocity, the relaxation time, and the wavenumber. The matrix sizes are too large for the analysis to cover all of the parameter space. Thus, numerical evaluation of the eigenvalues of the Jacobian stability matrix was performed for various parameter values to gain some understanding of the stability characteristics.

The main stability boundaries common to all three lattices are the following:

(1) A well-known stability boundary requires that the relaxation time be greater than one-half. Note that $\tau = \frac{1}{2}$ corresponds to zero shear viscosity. Since we are often interested in high Reynolds number flows, analysis is commonly performed along the stability boundary $\tau = \frac{1}{2}$.

(2) Another stability boundary requires the mean flow velocity to be below a maximum stable velocity that is a function of the other parameters.

(3) As τ is increased from one-half, the maximum stable velocity increases monotonically until a limit is reached. For the cases studied, the limit was around 0.39, 0.42, and 0.47 for the hexagonal, square, and cubic lattices, respectively.

These boundaries require all eigenvalues have an absolute value less than or equal to unity for all wavenumbers. Thus, numerical determination of the stability boundaries requires the determination of the most unstable wavenumber. As parameters are varied for the hexagonal lattice, the wavenumber that has the largest eigenvalue modulus changes considerably. Therefore, analysis was performed by sweeping through the entire range of wavenumbers while varying the other parameters. However, for the square and cubic lattices, the most unstable wavenumber was equal to 2.3 for values of τ near one-half.

One of the main results from this study is that for the hexagonal lattice there is a most stable value of the mass distribution parameter $\alpha = \frac{2}{3}$ which places two-thirds of the mass in the nonmoving population. For this value of α, the relaxation time τ was increased from one-half with the result that the maximum stable velocity increases monotonically with an asymptote for large τ around $\bar{\mathbf{u}} = 0.39$.

Both the square and cubic lattices provide stable behavior only when the values of the mass distribution parameters fall within certain ranges. A parametric relation between α and β can be selected which is consistently stable (for the mean flow velocity below some fixed value when $\tau > \frac{1}{2}$). Using this parametric relation, an important result of this study is that the maximum stable velocity is independent of α and, hence, β for a fixed τ. As τ is increased, as with the hexagonal lattice, the maximum stable velocity monotonically increases. However, when τ reaches some critical value, the most unstable wavenumber switches to a new eigenvalue that provides an upper limit on the maximum stable velocity equal to about 0.42 and 0.47 for the square and cubic lattices, respectively.

These results provide some stability guidelines for researchers using LB methods. The results provide a necessary condition for stability but the analysis does not include the effects of boundaries that may serve to destabilize simulations. Simulations performed too near the stability boundaries have been observed to go unstable. A common manifestation of instability is that as a given flow evolves, localized regions develop large velocities and instability ensues. We note that parameters resulting in stable flow consistently provide flow speeds and speeds of sound less than the lattice spacing divided by the time step. For this reason, a Courant stability condition is superceded by a

more stringent stability condition on the speeds. Another stability boundary common for finite-difference methods requires that the viscous diffusion speed be less than the lattice spacing divided by the time step. This boundary is not observed for LB methods because as the viscosity increases, errors of the scheme increase due to the presence of large nonequilibrium populations, but stability is still maintained.

As indicated in Section 2, the accuracy of the method for simulating the incompressible Navier–Stokes equations is expected to improve as the number of lattice sites is increased and as the Mach number is decreased. Quantification of these accuracy issues is presented in Ref. [21]. The result is that for models valid only in the incompressible-limit, the velocity should be small for both stability and accuracy. Note, however, that the time required for significant flow evolution (eddy-turnover time) is inversely proportional to the velocity so that one should select the maximum velocity that is both stable and provides compressibility errors within some desired level.

ACKNOWLEDGMENTS

We thank F. J. Alexander, M. G. Ancona, G. D. Doolen, D. W. Grunau, S. Hou, D. O. Martinez, W. H. Matthaeus, M. B. Reider, and Q. Zou for discussions and helpful suggestions. The work was supported by U.S. Department of Energy at Los Alamos National Laboratory. J.D.S. thanks G. Doolen, J. Rodgers, and the Center for Nonlinear Studies for sponsoring his stay in Los Alamos.

REFERENCES

1. D. H. Rothman, *Geophysics* **53,** 509 (1988).
2. S. Chen, K. Diemer, G. D. Doolen, K. Eggert, S. Gutman, and B. J. Travis, *Physica D* **47,** 72 (1991).
3. U. Frisch, B. Hasslacher, and Y. Pomeau, *Phys. Rev. Lett.* **56,** 1505 (1986).
4. K. Diemer, K. Hunt, S. Chen, T. Shimomura, and G. D. Doolen, "Density and Velocity Dependence of Reynolds Numbers for Several Lattice Gas Models," in *Lattice Gas Methods for Partial Differential Equations*, edited by G. D. Doolen (Addison–Wesley, Reading, MA, 1989), p. 137.
5. G. McNamara and G. Zanetti, *Phys. Rev. Lett.* **61,** 2332 (1988).
6. F. J. Higuera, S. Succi, and R. Benzi, *Europhys. Lett.* **9,** 345 (1989).
7. P. L. Bhatnagar, E. P. Gross, and M. Krook, *Phys. Rev.* **94,** 511 (1954).
8. J. M. V. A. Koelman, *Europhys. Lett.* **15,** 603 (1991).
9. S. Chen, H. Chen, D. Martinez, and W. Matthaeus, *Phys. Rev. Lett.* **67,** 3776 (1991).
10. Y. H. Qian, D. D'Humieres, and P. Lallemand, *Europhys. Lett.* **17,** 479 (1992).
11. A. J. Chorin, *J. Comput. Phys.* **2,** 12 (1967).
12. J. K. Dukowicz, Los Alamos Natl. Lab. Report, LA-UR-92-487, 1992 (unpublished).
13. J. D. Ramshaw and G. L. Mesina, *Comput. Fluids* **20,** 165 (1991).
14. F. J. Alexander, S. Chen, and J. D. Sterling, *Phys. Rev. E* **47,** 2249 (1993).
15. G. McNamara and B. Alder, *Physica A* **194,** 218 (1993).
16. Y. H. Qian and S. A. Orszag, *preprint* (unpublished).
17. Y. Chen, H. Ohashi and M. Akiyama, *Phys. Rev. E*, to appear.
18. J. E. Broadwell, *J. Fluid Mech.* **19,** 401 (1964).
19. T. Inamuro and B. Sturtevant, *Phys. Fluids A* **2,** 2196 (1990).
20. B. Nadiga and D. Pullin, *J. Comput. Phys.* **112,** 162 (1994).
21. M. B. Reider and J. D. Sterling, *Comput. & Fluids* **24,** 459 (1995).
22. M. Ancona, *J. Comput. Phys.* **15,** 107 (1994).
23. U. Frisch, D. d'Humieres, B. Hasslacher, P. Lallemand, Y. Pomeau, and J. P. Rivet, *Complex Systems* **1,** 649 (1987).
24. C. Bardos, G. Golse, and D. Levermore, *J. Statist. Phys.* **63,** 323 (1991).
25. W. G. Vincenti and C. H. Kruger, Jr., *Introduction to Physical Gas Dynamics* (Wiley, New York, 1965), p. 376.
26. H. Chen, S. Chen, and W. H. Matthaeus, *Phys. Rev. A* **45,** 5339 (1991).
27. D. O. Martinez, W. H. Matthaeus, S. Chen, and D. C. Montgomery, *Phys. Fluids A* **6,** 181 (1994).
28. S. Klainerman and A. Majda, *Phys. Lett. A* **120,** 229 (1987).
29. L. Kadanoff, G. McNamara, and G. Zanetti, *Phys. Rev. A* **40,** 4527 (1989).
30. G. McNamara, *private communication*.
31. R. Benzi, S. Succi, and M. Vergassola, *Phys. Rep.* **222,** 145 (1992).
32. D. W. Grunau, *private communication*.
33. S. Chen, Z. Wang, X. Shan, and G. D. Doolen, *J. Statist. Phys.* **68,** 379 (1992).
34. F. J. Alexander, S. Chen, and D. W. Grunau, *Phys. Rev. B, Rapid Commun.* **48,** R990 (1993).